International Journal of Remote Sensing

ISSN: 0143-1161 (Print) 1366-5901 (Online) Journal homepage: http://www.tandfonline.com/loi/tres20

Object-based image analysis of optical and radar variables for wetland evaluation

Laura Dingle Robertson, Douglas J. King & Chris Davies

To cite this article: Laura Dingle Robertson, Douglas J. King & Chris Davies (2015) Object-based image analysis of optical and radar variables for wetland evaluation, International Journal of Remote Sensing, 36:23, 5811-5841, DOI: 10.1080/01431161.2015.1109727

To link to this article: http://dx.doi.org/10.1080/01431161.2015.1109727

Published online: 23 Nov 2015.

International Journal of Remote Sensing, 2015
Vol. 36, No. 23, 5811–5841, http://dx.doi.org/10.1080/01431161.2015.1109727

Taylor & Francis
Taylor & Francis Group

Object-based image analysis of optical and radar variables for wetland evaluation

Laura Dingle Robertson[a]*, Douglas J. King[a], and Chris Davies[b]

[a]*Department of Geography and Environmental Studies, Geomatics and Landscape Ecology Research Lab, Carleton University, Ottawa, Ontario, Canada K1S 5B6;* [b]*Ontario Ministry of Natural Resources, Trent University, Peterborough, Ontario, Canada K9J 7B8*

(*Received 8 March 2015; accepted 24 September 2015*)

Optical and radar imagery has been shown to be useful for classifying wetland types and surrounding non-wetland classes such as forest and agriculture. Throughout the literature, recommendations have been made that optical and radar image variables together should improve overall and individual class accuracies. object-based image analysis (OBIA) uses multiple data types to segment objects representing land cover entities that are subsequently classified. There are few studies that have utilized optical and polarimetric radar variables together in OBIA to map wetland classes. This research investigated the potential to combine WorldView-2 optical image variables with fully polarimetric Radarsat-2 image variables in OBIA classification of wetland type. With the addition of radar polarimetric variables, classification accuracy improved for the wetland classes of fen, bog, and swamp over the use of optical imagery alone; specifically the addition of Cloude–Pottier (CP) variables of entropy, anisotropy, and alpha angle improved the classification of fen, and the addition of horizontal transmit and horizontal receive (HH) and horizontal transmit and vertical receive (HV) backscatter intensity improved the classification of swamp.

1. Introduction

For wetland analysis and mapping, optical imagery has been shown to be useful in classifying wetland types (e.g. bog, fen, marsh, swamp) (Dronova et al. 2012; Zhang et al. 2011; Belluco et al. 2006), delineating water and land boundaries (Rivero et al. 2009), and deriving biophysical parameters such as biomass (Mutanga, Adam, and Cho 2012; Dillabaugh and King 2008), among others.

Radar remote sensing can also be used to identify wetlands and wetland characteristics. It has been shown to detect herbaceous wetlands (Pope et al. 1997) and to indicate standing snags in open swamps or emergent vegetation (e.g. reeds) (Karszenbaum et al. 2000; Kandus et al. 2001). Multi-polarized radar has been shown to be better correlated than single polarizations with soil moisture and inundation (Lang and Kasischke 2008; Dobson and Ulaby 1988), and many wetland types (bog, fen, saline, and freshwater marsh, etc.) have been discriminated (Evans et al. 2014; Marechal et al. 2012; Lu and Kwoun 2008; Li and Chen 2005; Racine, Bernier, and Ouarda 2005). Polarimetric decomposition variables have been used to categorize wetland types (Touzi, Deschamps, and Rother 2007), map macrophyte species (Sartori et al. 2011), and indicate flooded vegetation (Schmitt and Brisco 2013). Relationships between C-band horizontal transmit and horizontal receive (HH) and vertical transmit and vertical receive (VV)

*Corresponding author. Email: laura.dinglerobertson@carleton.ca

backscatter and soil moisture and inundation have been found to be positive and linear (Lang and Kasischke 2008). Several studies have utilized a graphical relationship of polarization response at various incidence angles to discriminate wetland type classes (Marti-Cardona et al. 2010; Horritt et al. 2003; Baghdadi et al. 2001).

Throughout the literature it has been suggested that combining optical and radar imagery should improve overall and individual class accuracies (Adam, Mutanga, and Rugege 2010; Silva et al. 2008; Henderson and Lewis 2008; Ozesmi and Bauer 2002; Kasischke, Melack, and Dobson 1997). However, to date most studies have assessed wetlands using either optical or radar imagery.

Object-based image analysis (OBIA) is one technique that can use multiple data types to create objects of land cover entities which can then be classified. In previous research it has been found that OBIA classifications are better representations of land cover entities as humans perceive them than pixel-based classifications (Meneguzzo, Liknes, and Nelson 2013; Pasher et al. 2013; Brenner, Christman, and Rogan 2012; Dronova et al. 2012; Duro, Franklin, and Dube 2012; Dingle Robertson and King 2011; Burnett and Blaschke 2003). OBIA has been used with optical imagery to map salt marsh plants and to derive vegetation zones, patches, and surface water channels (Moffett and Gorelick 2013; Ouyang et al. 2011). Dingle Robertson and King (2011), in a precursor to this study, evaluated Landsat OBIA and pixel-based land cover maps in temporal analysis of land cover change, including for wetlands.

OBIA has been used with radar imagery, including fully polarimetric data, to map water/land boundaries and wetland types (Evans and Costa 2013; Li et al. 2012). It has also been used with optical imagery combined with single polarized radar imagery (e.g. RADARSAT-1, JERS-1) to map wetland types (Durieux et al. 2007; Grenier et al. 2007) and to map the temporal variability in aquatic plant communities (Silva, Costa, and Melack 2010). Only a few studies have utilized both optical image variables and fully polarimetric radar variables together with OBIA to assess wetland type classes, albeit at different wavelengths and spatial resolutions (e.g. ALOS PALSAR L-band radar decomposition variables with AVHRR surface temperature and NDVI from ENVISAT MERIS (Dabrowska-Zielinska et al. 2009); S- and X-band airborne radar decomposition variables with NDVI from Landsat TM/ETM+ and very high-resolution aerial imagery (Van Beijma, Comber, and Lamb 2014); ALOS PALSAR L-band with very high-resolution four band aerial imagery (30 cm to 50 cm) (Kloiber et al. 2015); and TerraSAR-X radar imagery with Landsat TM, KOMPSAT-2, MODIS, and aerial optical imagery (Muster et al. 2013).

Given the known spectral reflectance and microwave backscatter responses to vegetation composition and structure variations that are associated with major wetland types, and the tendency of vegetation communities in each wetland type to be spatially distributed as distinct entities, the objective of this research was to determine if combining high-resolution WorldView-2 optical and polarimetric Radarsat-2 image variables in OBIA would result in improved overall land cover classification accuracy and an improvement in the accuracy of individual wetland types. This article is part of a larger study on assessment of wetlands using remote sensing and GIS within the Ontario Wetland Evaluation System (OWES) as summarized in Dingle Robertson (2014).

2. Study areas

This research was carried out in eastern Ontario, Canada (Figure 1), a spatially diverse region of approximately 15,500 km^2 including agricultural, forest, and urban lands.

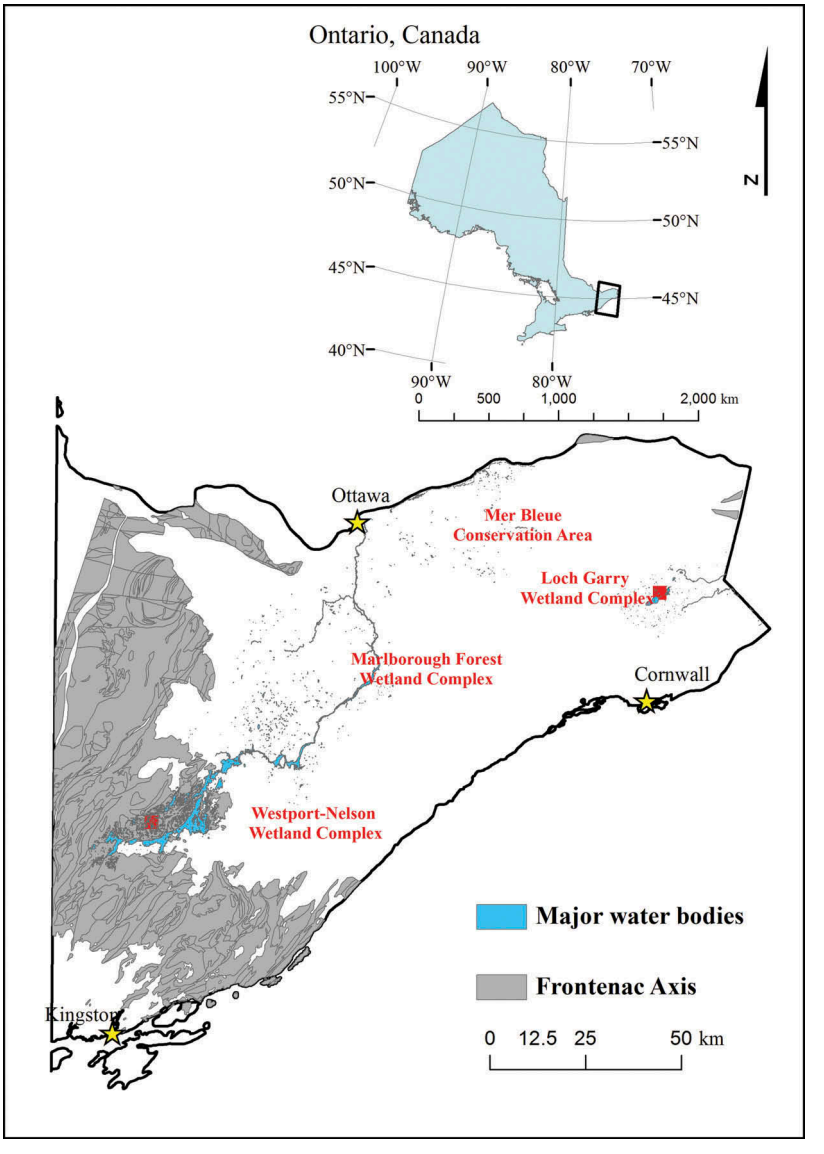

Figure 1. Eastern Ontario and the position of the four wetland complex study areas (red squares).

Wetland complexes are distributed throughout the region and predominantly contain swamps and marshes with fewer bogs and fens. For the purposes of this research, the Canadian National Wetlands definitions were used (excluding shallow water) (National Wetlands Working Group 1997). Bog includes: peat-covered areas and/or peat-filled depressions; a surface carpet of mosses (*Sphagnum* spp.); closed drainage, strongly acidic surface waters, and peat; and it is treed or treeless (tree cover does not exceed 25%). Fen includes: poorly to moderately decomposed peat; mosses with narrow pH tolerance (sphagnum may or may not be present); a dominant component of sedges (*Carex* spp.) with grasses (*Poaceae* spp.), and reeds (*Phragmites* spp.) in local pools; often low- to medium-height shrub cover or sparse tree cover (white cedar (*Thuja*

occidentalis L), tamarack (*Larix laricina* (Du Roi) K.Koch)); water and peat that are less acidic than bogs; and a layer of shrubs from the heather family (*Ericaceae* spp.). Swamps include: wooded wetlands (≥25% cover of trees and tall shrubs); standing to gently flowing water (pools and channels indicate subsurface flow); characteristic flooding in spring with relic pools later in summer; sometimes with a significant low shrub community, but a tall shrub component must be present/dominant. They can be subclassified as treed swamps or shrub swamps; treed swamps include conifer swamps (white cedar, tamarack, black spruce (*Picea mariana* (Mill.) Britton, Stems & Poggenburg)) and deciduous swamps (silver maple (*Acer Saccharinum* L.), elm (*Ulmus* L.), black ash (*Fraxinus nigra* Marshall), and yellow birch (*Betula alleghaniensis* Britt.)). Marshes include: non-woody emergent vegetation (rushes (*Juncus* spp.), reeds (*Typha* spp.), sedges with anchored floating plants) and submergent vegetation; wet areas that are periodically and/or permanently inundated; and zones/mosaics of vegetation that are interspersed with channels or pools of water. Although variability between study areas was present, Figure 2(*a*)–(*d*) shows examples representing typical conditions in bog (*a*), fen (*b*), marsh (*c*), and swamp (*d*).

Four wetland complexes were selected for study including Loch Garry Wetland Complex ('Loch Garry'), Marlborough Forest Wetland Complex – which, despite being called a forest has large areas of marsh, fen, and swamp present

Figure 2. Photographic examples representing typical conditions in bog (*a*), fen (*b*), marsh (*c*), and swamp (*d*).

('Marlborough'), Mer Bleue Conservation Area ('Mer Bleue'), and Westport-Nelson Wetland Complex ('Westport') (Figure 1). These cumulatively represented approximately 6200 ha. Multiple wetland complexes were selected to represent the diversity of conditions across eastern Ontario. Previous studies have generally been limited to one or two wetlands or wetland complexes (e.g. Van Beijma, Comber, and Lamb 2014; Dronova et al. 2012; Ricaurte et al. 2012; Jiao et al. 2011; Castaneda and Ducrot 2009; Durieux et al. 2007; Grenier et al. 2007; Touzi, Deschamps, and Rother 2007; Wright and Gallant 2007; Li and Chen 2005; Bernier et al. 2003), leading to questions about the potential for spatial extension of the results, while few studies have attempted to concurrently analyse and compare classifications from multiple wetland complexes (e.g. Mwita et al. 2013).

Situated north of Cornwall, Ontario, Loch Garry is found within fragmented farmland and located along the shores of a large lake, which is 1 to 5 m deep and covers about 3.8 km^2 (380 ha). The wetland complex is about 1281 ha within the Garry River watershed (3400 ha), and contains three wetland types: fen, marsh, and swamp. The lake is hydrologically isolated, with water being supplied to the Garry River watershed through precipitation.

Marlborough is approximately 1099 ha in area and is located southwest of Ottawa, within less fragmented farmland but near industrial land uses (e.g. quarrying). It is comprised of swamp, marsh, and fens containing rare orchid species. This complex is recreationally active with extensive hunting, all-terrain vehicle, and snowmobile use.

Mer Bleue is within the city limits of Ottawa, with extensive suburban development to the north and surrounded by farmland to the south and east. This well-studied area of approximately 3500 ha is a wetland complex of international importance (Ramsar, 2006). The bog area is approximately 7700 years old and representative of a northern boreal landscape, including flora and fauna species that are common to boreal bogs. There are also extensive marshes located in this area.

Westport is located on the Frontenac Axis, approximately 120 km southwest of Ottawa and 60 km north of Kingston. The axis is an extension of the Canadian Shield that divides the St. Lawrence lowlands and the Great Lakes lowlands. Bedrock is often exposed at the surface, or covered with thin soils (Keddy 1995). The area was forested in the past, but logging has depleted most areas of old-growth (Keddy 1995).

3. Data

Table 1 lists details of the high-resolution WorldView-2 and Radarsat-2 imagery used in this research. A generalized description of these imagery types and justification for their selection follows.

WorldView-2 imagery was selected for detailed, high-resolution within-wetland complex analysis and mapping. The nominal ground pixel size is 46 cm and 1.8 m for the PAN (panchromatic) band and the four multispectral bands, respectively, over an image area of approximately 18 km × 18 km. The spectral bands were blue-green (450–510 nm), green (510–580 nm), red (630–690 nm), and NIR (770–895 nm). Additional spectral bands available with Worldview-2 were not used due to higher cost and because it was not certain whether they would provide additional non-redundant information since spectral bands within the same portion of the spectrum are commonly highly correlated. The data were delivered corrected to the world geodetic survey 1984 datum (WGS84) and the Universal Transverse Mercator (UTM) coordinate system (zone 18,

Table 1. Imagery used in this research including season, date acquired, and details related to the type of imagery.

Date	Image type	Site (s)	Details	Incidence angle, ° (Near–Far)	No. of rows and columns	Extent (km × km)	Nominal ground pixel size (m × m)
SPRING	Radarsat-2	Marlborough	Fine Quad (FQ)1	18.4–20.4	1761 × 7215	25.0 × 35.0	14.2 × 4.9
29 March 2010							
9 April 2010			FQ 29	46.8–48.0	4256 × 6679	27.3 × 31.7	6.4 × 4.8
8 April 2010		Westport	FQ 7	25.7–27.6	2588 × 6005	27.2 × 28.5	10.5 × 4.8
25 April 2010	WorldView-2	Loch Garry					
25 April 2010		Mer Bleue					
17 May 2010		Marlborough					
28 April 2010		Westport					
SUMMER	Radarsat-2	Loch Garry	FQ 10	29.1–30.9	2889 × 5094	26.0 × 27.0	9.0 × 5.3
23 June 2010							
26 June 2010		Mer Bleue	FQ 7	25.7–27.6	2588 × 6238	27.0 × 29.5	10.4 × 4.7
2 August 2011			FQ 28	46.0–47.2	4208 × 5856	27.0 × 27.5	6.4 × 4.7
3 July 2010		Marlborough	FQ 5	23.4–25.3	2372 × 5867	27.0 × 29.0	11.4 × 4.9
26 June 2010		Westport	FQ 2	20.0–21.8	2060 × 6088	27.4 × 29.6	13.3 × 4.9

row T). The accuracy of these corrections was assessed using the Ontario road vector file and control points at road intersections. The images were aligned to an Ontario road vector file using a first-order polynomial transformation and nearest neighbour resampling, resulting in an overall root mean square positional error (RMSE) of less than ½ pixel.

Radarsat-2 is a C-band sensor with advanced polarimetric capabilities and multiple possible resolutions and image swaths that have proven advantageous in wetland mapping (Henderson and Lewis 2008; Touzi, Deschamps, and Rother 2007). Polarimetric radar detects the polarization properties of a surface. Surfaces respond to incident polarized radiation by reflecting partially polarized and depolarized radiation (Van Zyl, Zebker, and Elachi 1987). Fully polarimetric radar systems measure surface characteristics for all configurations (e.g. HH, VV, HV, VH). By distinguishing between different surface characteristics, they improve upon data acquired in single polarizations. Stokes parameters describe the polarization state and phase. Coherency matrices are the second-order statistical representation of the variations and correlations of that polarization state and phase (Van Zyl, Zebker, and Elachi 1987).

Radarsat-2 imagery was acquired in descending mode in fine quad-polarization. Steep-incidence angle imagery was desired to discriminate between wetland types based on previous study results (Baghdadi et al. 2001). However, multiple angles were acquired to test the effect of incidence angle on wetland type discrimination under the diverse wetland conditions of this study. The nominal ground pixel size is theoretically 8 m at the steepest incidence angle (18.4°) and was therefore expected to be larger than this for the images shown in Table 1. In two cases, very shallow angle imagery (FQ 28, 29) was acquired when other prioritized organizations needed steep-angle imagery. Lower FQ numbers (e.g. 1, 2) relate to steeper incidence angle-acquired data, and higher FQ numbers (e.g. 28, 29) relate to shallower incidence angle-acquired data.

A 10 m digital elevation model (DEM, Version 2.0.0, horizontal accuracy ±10 m; vertical accuracy ±5 m, Land Information Ontario (LIO), Ontario Ministry of Natural Resources (OMNR), 2006) was also obtained; although eastern Ontario is relatively flat (less than 200 m change across the region). It was thought that the addition of elevation data may indicate a difference for certain wetland types (e.g. raised bog or marshes downslope of upland).

4. Methods

4.1. Field validation data acquisition

In the spring and summer of 2010 and 2011, validation sites of approximately 90 m × 90 m were established in the four study areas to obtain representative samples of each of the wetland and non-wetland land cover types. This site size was selected to represent about 3 × 3 Landsat pixels as Landsat 5 TM data were used in the broader study described in Dingle Robertson (2014). A visual survey was made of the land cover types present at each site and a global positioning system (GPS) waypoint was taken at the edge of the site using a Trimble Juno SB (expected real time accuracy of approximately 2–5 m (www.trimble.com 2013)). Efforts were made to accumulate multiple samples for each land cover type (e.g. 15–50 (Foody 2002)), but for the rarer wetland types of fen and bog it was often impossible to find more than one or two spatially disparate examples within a particular wetland complex. All four wetland types were also not observed, nor known to exist from previous OWES surveys in the wetland

complexes. Eighty-five wetland sites were observed in the field (18 bog, 11 fen, 37 marsh, and 19 swamp) and an additional 71 field sites of upland and water were also recorded.

4.2. Extraction of radar image variables

A 7 × 7 enhanced Lee adaptive filter was applied to the raw radar data to reduce speckle while maintaining edges or sharp features in the image. This filter and window size were selected following De Leeuw (2009), who found that they outperformed about 20 other speckle filter/window size combinations and had speckle reduction rates up to 70%.

The radar backscatter coefficient is an indication of the average backscattered power in relation to the incident power and is represented as σ^o, measured in decibels (dB) (Ulaby, Haddock, and Austin 1988). HV and HH σ^o images were derived from the acquired radar images and samples were extracted at field validation locations for all land cover types at all study areas. These data were plotted on scatter graphs to determine whether wetland type could be distinguished based upon HH and HV backscatter.

Several methods have been developed to extract different representations (variables) of scattering mechanisms from the coherency matrix (Liao and Wang 2010) of polarimetric radar data. These variables can then be used in land cover classification. One common method is the Cloude–Pottier (CP) decomposition (Schmitt and Brisco 2013; Sartori et al. 2011; Liao and Wang 2010; Touzi, Deschamps, and Rother 2007; Cloude and Pottier 1997, 1996). Targets contain not only radar response but speckle (noise) and random scattering (from surface and volume components); therefore analysis to determine the underlying scattering properties of the target requires a multivariate statistical description through matrix mathematics (Cloude and Pottier 1996). The resultant CP variables entropy, anisotropy, and alpha angle relate to the target surface, volume, and double-bounce/multiple scattering mechanisms.

Entropy (H, range = 0–1) represents the degree of randomness. $H = 0$ indicates a non-depolarizing scattering process and generally relates to one dominant scattering mechanism, while $H = 1$ relates to depolarizing surfaces (Liao and Wang 2010; Cloude and Pottier 1997, 1996). Low entropy is expected for open water and a marsh/water combination that is dominated by surface scattering. Entropy is expected to increase with increasing vegetation structural complexity; medium entropy was expected to represent bog and fen vegetation, and high entropy was expected to represent swamp and upland vegetation (Touzi, Deschamps, and Rother 2007).

Anisotropy (A, range = 0–1) is a measure of the difference between the second and third scattering mechanisms. When $A = 0$ the two mechanisms are mixed in equal proportions and when A is close to 1, the second scattering mechanism is dominant over the third. This provides information complementary to entropy and allows for interpretation of the relative contributions of the types of scattering mechanism. For example, low anisotropy with high entropy may be indicative of both volume and double-bounce scattering mechanisms as found with swamps (Sartori et al. 2011; Touzi, Deschamps, and Rother 2007)

Alpha angle (α) identifies the dominant scattering mechanism (Cloude and Pottier 1997). Low α values (0–40º) indicate surface scattering, medium values (40–52.5º) are representative of volume scattering, and high values (e.g. close to 90º) indicate double-bounce/multiple scattering (Banks et al. 2014; Liao and Wang 2010; Cloude and Pottier

1997, 1996). Dense canopies of grasses and sedges result in mean alpha close to 45° and are representative of predominantly volume scattering (Sartori et al. 2011).

The backscatter images (HH, HV, VV) and the three CP decomposition variable images were geo-corrected using NEST4C-1.1 (European Space Agency) allowing for spatial cross-referencing to the validation data, and for use in segmentation and classification with the geo-corrected optical imagery.

4.3. *Object-based image analysis*

OBIA has two key processing steps: 1) segmenting imagery and other ancillary data into objects representing relative spatial homogeneity; and 2) classifying the segmented objects as land cover classes of interest. OBIA for wetland type classes was completed using eCognition Developer 64 (8.64) (segmentation) and IDRISI Taiga (C4.5 decision tree classification (Quinlan 1990)).

4.3.1. *Segmentation of objects*

The technical objective in segmentation is to define objects that have minimized within-object variability and maximized between-object variability. The creation of objects from individual pixels is based upon the spectral and spatial properties of neighbouring pixels (Burnett and Blaschke 2003). Multi-resolution segmentation was selected for this research, as Marpu et al. (2010) showed that this algorithm was one of the two best from a comparison of 12 segmentation algorithms in terms of positional accuracy of segmented boundaries of land cover objects. Data input to the segmentation process included the four Worldview-2 spectral bands and the DEM. Tests with the addition of the radar variables in the segmentation process did not improve upon, or refine, the overall selection of the segmentation parameters. Therefore, radar image variables were not included in the segmentation testing stage.

The key parameter in multi-resolution segmentation is a unit-less variable of 'scale' that is related to the image pixel size. Additional parameters of 'colour' (the pixel value (e.g. DEM; spectral band brightness) and 'shape' (the geometric characteristics of the segmented features (Laliberte et al. 2004), which is further defined by boundary 'smoothness' and feature 'compactness'), were also tested.

To determine the best scale, shape, and compactness values, most studies have followed a 'trial and error' process using visual comparison of how well the segmented object boundaries align with interpreted objects (Aguilar, Saldana, and Aguilar 2013; Duro, Franklin, and Dube 2012; Dingle Robertson and King 2011; Ouyang et al. 2011). More recently, multiple Estimation of Scale Parameter (ESP) tools have been developed (e.g. Dragut, Tiede, and Levick 2010) although they have not been widely used in the literature.

This research followed the 'trial and error' process, first for the scale parameter by assessing the alignment of segmented wetland object boundaries with the water/land interface, and of the alignment of segmented roads and fields with their visible edges in the imagery. Additionally, test classification accuracies at a variety of scale values (with unchanging shape and compactness values) were also compared. This analysis resulted in the selection of an optimal scale parameter value of 45. In addition to image pixel size, the size of the scale parameter is closely related to the class of interest. In the overall research, (Dingle Robertson 2014) where more detailed classes such as vegetation community forms or open water-type configuration were also investigated, smaller-

Table 2. Experimental design matrix showing shape/colour and compactness/smoothness tests implemented after Tian and Chen (2007).

	Compactness parameter (Compactness + Smoothness = 1.00)			
Shape (1.00 – Colour)	0.25	0.50	0.75	0.90
0.10	Test 1	Test 2	Test 3	Test 4
0.25	Test 5	Test 6	Test 7	Test 8
0.50	Test 9	Test 10	Test 11	Test 12
0.75	Test 13	Test 14	Test 15	Test 16
0.90	Test 17	Test 18	Test 19	Test 20

scale values (e.g. 25) related to those specific class types rather than the coarser overall class types of fen, bog, marsh, and swamp. For the selected scale value of 45, following Tian and Chen (2007), an experimental design matrix (Table 2) was used to visually evaluate segmentation results for each combination of the shape and compactness parameter values. From these tests, the optimal OBIA parameter values were determined as scale value = 45, shape value = 0.1, compactness value = 0.75.

4.3.2. *Training data*

For the classes of bog, fen, marsh, swamp, upland, and water, segmented objects selected for classifier training were representative of the class spectral and/or spatial characteristics at each study area. Training objects were selected using the field observation information. For the uplands class, when multiple and spectrally different upland class types existed adjacent to a wetland (e.g. forest, agricultural, urban), training was conducted separately for each specific class. Following classification, these classes were merged into a single upland class.

4.3.3. *Classification of segmented objects*

Classification of the segmented objects was conducted using a classification tree technique (hereafter called classification tree analysis, CTA). Classification trees are nonparametric and do not require assumptions regarding data distributions (Friedl and Brodley 1997). Splits in the tree are determined through recursive partitioning of the training data, where at each node the data are split until the remaining data are only from one class or there is one acceptable level of class dominance (this endpoint being a leaf in the decision tree). A commonly used algorithm is C4.5 (Quinlan 1990), which is a univariate classifier with three splitting options (entropy, gain ratio, and GINI index). Although there are alternative CTA algorithms available in other software packages, research has shown that the type of CTA algorithm has little effect on the overall classification accuracy (Zambon et al. 2006).

Research has also found that, in general, there is no statistical difference between the splitting techniques; however, through testing, others have recommended use of the GINI index (Duro, Franklin, and Dube 2012; Zambon et al. 2006). The GINI index measures the impurity at a given node, which is at a maximum when all the pixels at the node are equally distributed among all classes. The main splitting criterion is the reduction of that impurity. This index is defined as

$$\mathrm{GINI}(t) = \sum_i p_i(1 - p_i), \tag{1}$$

- where p_i is the proportion of class i at node t, determined by dividing the total number of observations of class i by the total number of observations; and
- t represents any node (parent or child) at which a given split of the data is performed (Apte and Weiss 1997).

The classifier starts by finding the two largest homogenous groupings within a data set and isolates them as nodes. Subsequently, nodes are then iteratively split in the same manner until further divisions are not possible (Zambon et al. 2006). Auto-pruning was set at 1%, which removes any leaves with pixel counts less than or equal to 1% of the total number of training pixels.

4.3.4. *Classification accuracy assessment*

The reference data samples were split into training and validation sets in a ratio of 30:70%, respectively (McCoy 2005; Foody 2002). Thematic map accuracies were assessed using error matrices that compare validation data with the classification data and their associated measures of producer's accuracy (PA = 100% minus the percentage errors of omission) and user's accuracy (UA = 100% minus the percentage errors of commission) (Foody 2002; Congalton and Green 1993). The kappa coefficient (κ) of agreement, which indicates the accuracy of the map beyond that which would be obtained through a random assignment of pixels to land cover classes, was also used (Foody 2002; Congalton and Green 1993). For all OBIA classifications, because the objects had been rasterized, the accuracy assessments were based upon selection of a single pixel sample per validation object within the 90 m × 90 m (or larger) field-assessed area (i.e. only one sample per validation object was used to maximize spatial independence between samples). As the validation data are based on objects, and each sample represented a field-visited location, the total number of samples was limited by fieldwork time and access. The 30:70% ratio ensured a sufficiently large representative training set, while maintaining a representative validation portion to generate accuracy statistics.

5. Results

In the following sections, graphical (Figures) results are provided for example study areas, with numerical (Tables) results provided for all areas.

5.1. Segmentation and classification of wetland type using optical imagery spectral variables and elevation

As an example of the segmentation results, Figure 3(*a*), shows the objects created for the Loch Garry wetland complex using the spring 2010 WorldView-2 image and elevation as inputs with the optimal parameter values of scale = 45, shape = 0.1, and compactness = 0.75. In Figure 3(*b*) the red outline shows the objects forming the boundary of a known fen. Figure 3(*c*) shows the objects that follow a known water channel and Figure 3(*d*) shows the objects following the shoreline of the lake, Loch Garry. The lake is comprised of several objects instead of just one; this represents the

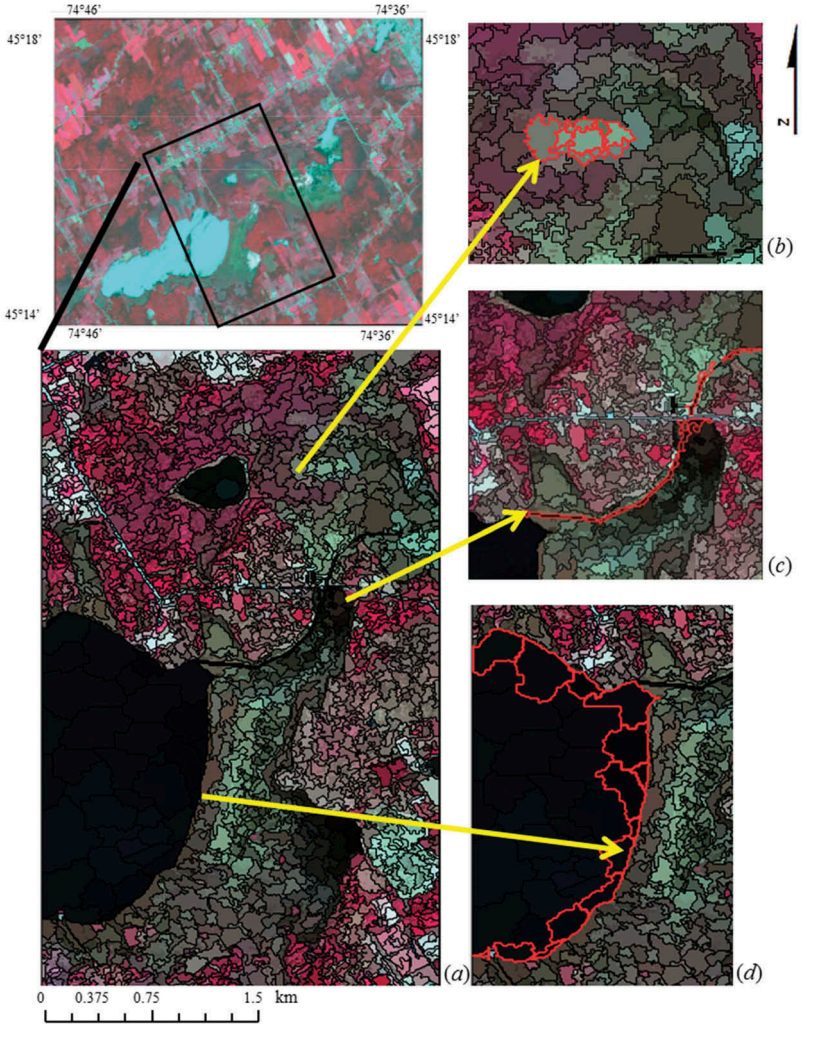

Figure 3. (*a*) Colour infrared (CIR) composite of the spring 2010 Loch Garry subset showing the created objects using a scale value of 45, shape value of 0.1, and compactness value of 0.75; and in red (*b*) objects that make up the boundaries of a known fen; (*c*) objects that form a known channel; and (*d*) objects that mimic the shoreline of Loch Garry.

qualitative aspect of the scale parameter choice where certain features (for example, a large lake) may be over-segmented in order to capture smaller features of interest (for example, the water channel in Figure 3(*c*)). The choice of scale parameter value is highly dependent upon the importance of particular features to the research.

Figure 4 presents the Loch Garry CTA based on the optical imagery and DEM. Areas that were observed in the field and were well classified (red circles) include the water channel in the centre, the small lake to the northwest, and the shoreline of Loch Garry. Known swamp areas around the lake in the northern part of the map and at the edge of the upland in the southeast were well classified. Similarly, the large fen on the east side of the lake was correctly classified.

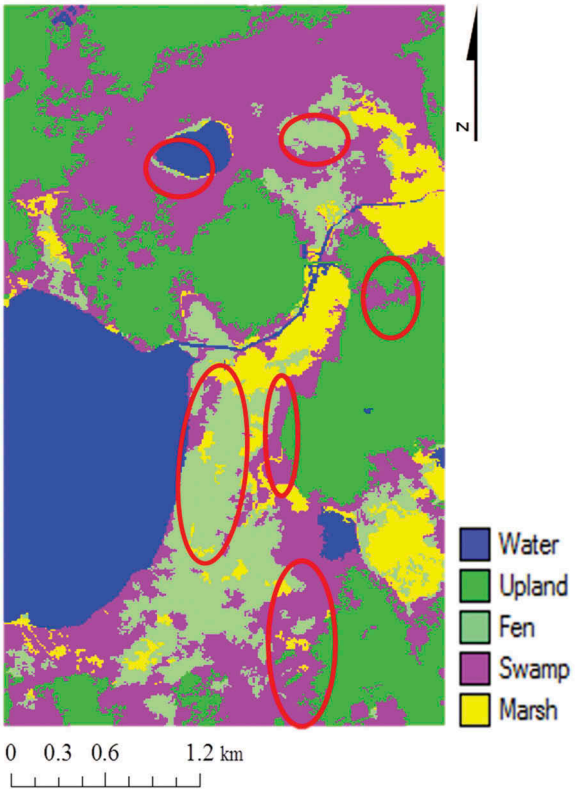

Figure 4. Object-based CTA thematic classification of Loch Garry derived using 2010 spring WorldView-2 and DEM data. Red circles show wetland areas that were well classified (confirmed in the field). The map coverage corresponds to the area shown in Figure 3(*a*).

The total wetland area assessed in the last OMNR Loch Garry field-based evaluation in 1983 was 543 ha, while the total wetland area classified using the CTA was 435 ha. Percentage cover estimates by class were: fen 23% (CTA) and 14% (field); swamp 62% (CTA) and 40% (field); and marsh 15% (CTA) and 46% (field). Overall, the CTA extents for swamp and fen were greater than the 1983 field-based OMNR assessment while CTA marsh area was smaller. These differences could be related to wetland dynamics over the ~28-year period; it is possible that marsh areas gradually filled in with shrubs and trees to become swamp. For fen, the increases are harder to justify; they could be related to encroachment of fen on Loch Garry. The differences for all classes could also be related to the viewpoint from which the field-based observers made their observations (obliquely and subject to spatial distortions) as compared to remote sensing (vertically).

Table 3 shows the classification error matrix and accuracy statistics. The overall accuracy was 86.5% with $\kappa = 0.82$. The average PA was 87.3% and the average UA was 91.7%. Water was the most accurately classified while marsh and swamp were the worst classes in terms of PA and UA, respectively. The small sample size of the object-based validation set means there is a degree of imprecision expected (potentially large confidence intervals) in these results. However, field knowledge supports these classification results, as larger areas were not erroneously classified.

Table 3. Error matrix and accuracy statistics for the spring 2010 Loch Garry object-based CTA.

		Reference samples					
Classified samples		Water	Upland	Fen	Swamp	Marsh	Total
	Water	5	0	0	0	0	5
	Upland	0	13	0	0	0	13
	Fen	0	0	4	0	0	4
	Swamp	0	3	1	7	1	12
	Marsh	0	0	0	0	3	3
	Total	5	16	5	7	4	37
		PA/UA (%)					Average (%)
Overall accuracy (%):	86.5	100.0/	81.3/	80.0/	100.0/	75.0/	87.3/
Overall κ:	0.82	100.0	100.0	100.0	58.3	100.0	91.7

Table 4 provides the classification accuracies for all four wetland complex study areas (Loch Garry repeated from above) as derived using the optical and DEM data. The area with the highest overall accuracy was Loch Garry (86.5%) and the area with the lowest accuracy was Marlborough (70.0%). Over the four wetland complexes, fen had the highest average PA (90.0%) and UA (75.0%) while bog had the lowest (PA = 65.9%; UA = 50.3%). In relation to the literature for wetland type classification, these results were comparable, as they fell within the typical overall accuracies of 71–92% (Evans et al. 2014; Schmitt and Brisco 2013; Dribault, Chokmani, and Bernier 2012; Ricaurte et al. 2012; Dronova, Gong, and Wang 2011; Jiao et al. 2011; Waleska et al. 2011; Castaneda and Ducrot 2009; Durieux et al. 2007; Grenier et al. 2007; Touzi, Deschamps, and Rother 2007; Wright and Gallant 2007; Li and Chen 2005; Racine, Bernier, and Ouarda 2005; Bernier et al. 2003).

5.2. *Radarsat-2 data analysis*

HV and HH backscatter intensity was extracted at field validation locations for upland, fen, bog, marsh, and swamp at all four wetland study areas and for all incidence angles (ranging from steep to shallow (18.4º to 48.0º, respectively)). An assessment of season was conducted where data were available. As an example of the differences between wetland as a generalized class and upland, Figure 5 shows a comparison for the spring and summer steep-incidence angle 2010 Marlborough Radarsat-2 imagery. It can be seen that there is better distinction between wetland and upland in spring as compared with summer. This is not surprising as the greater coverage of standing water following snow melt in spring would be expected to contribute to higher backscatter from vegetation–water double-bounce interactions (Touzi et al. 2004; McNairn et al. 2002; Boerner et al. 1998; Evans et al. 1988).

Given that spring imagery was determined to discriminate wetlands from upland better than summer imagery, the next step was to evaluate incidence angle in wetlands for which steep and shallow spring imagery were available. Figure 6 shows that in Marlborough there is greater overlap between classes at shallower incidence angles (Figure 6(*b*)) than at steeper angles (Figure 6(*a*)). Bog was not included in this analysis as it was not present in Marlborough. However, as can be seen in Figure 7 with summer imagery for Mer Bleue, there is also greater overlap in the shallower-incidence angle imagery (Figure 7(*b*)) than at steeper angles (Figure 7(*a*)) (comparison is completed with

Table 4. Accuracy statistics for object-based CTA using 2010 spring Worldview-2 optical and DEM data at all four study areas.

			Water		Upland		Fen		Bog		Swamp		Marsh		Average	
	Overall accuracy (%)	κ	PA (%)	UA (%)	PA (%)	UA (%)	PA (%)	UA (%)	PA (%)	UA (%)	PA (%)	UA (%)	PA (%)	UA (%)	PA (%)	UA (%)
Loch Garry	86.5	0.82	100.0	100.0	81.3	100.0	80.0	100.0	n/a	n/a	100.0	58.3	75.0	100.0	87.3	91.7
Marlborough	70.0	0.60	83.3	100.0	60.0	64.3	100.0	50.0	n/a	n/a	60.0	64.3	63.6	70.0	78.1	71.1
Mer Bleue	73.2	0.64	100.0	100.0	77.8	93.3	n/a	n/a	60.0	60.0	n/a	n/a	62.5	100.0	72.1	76.1
Westport	72.5	0.65	100.0	75.0	75.0	66.7	n/a	n/a	77.8	63.6	n/a	n/a	63.6	77.8	73.3	76.6
Average Accuracy (%) over all four wetlands	75.5	0.68	95.8	93.7	68.8	84.8	90.0	75.0	65.9	50.3	80.0	61.3	66.2	83.0	77.7	78.9

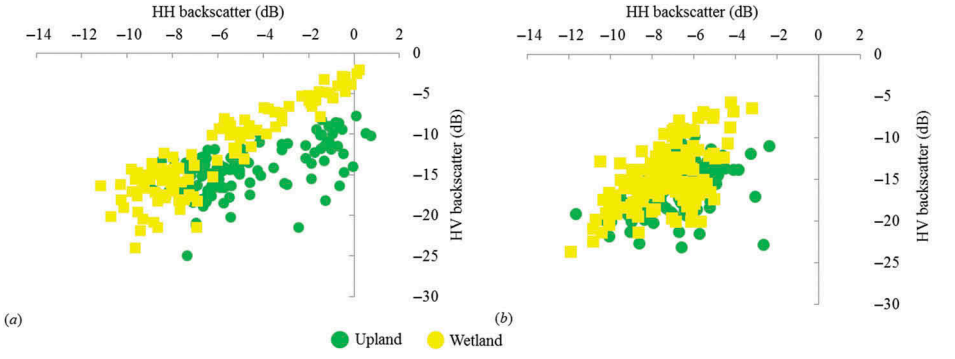

Figure 5. Marlborough 2010 steep-incidence angle Radarsat-2 backscatter for upland (green) and wetland (yellow) for (*a*) spring and (*b*) summer.

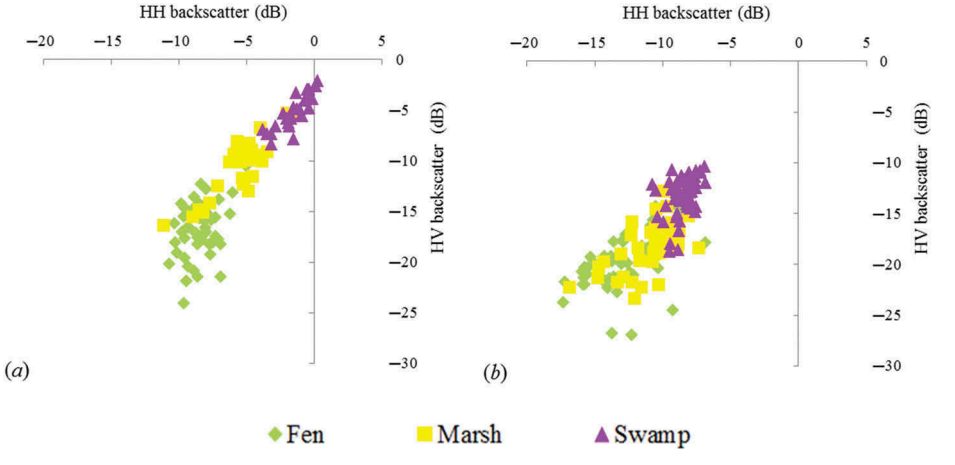

Figure 6. Marlborough spring 2010 Radarsat-2 backscatter for fen (green), marsh (yellow), and swamp (purple) at (*a*) steep (18.4–20.4°) and (*b*) shallow (46.8–48.0°) incidence angles.

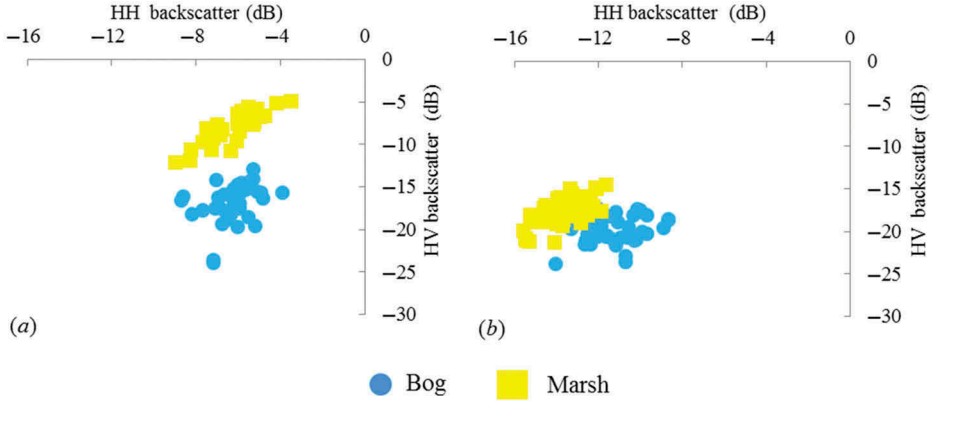

Figure 7. Mer Bleue summer 2010 Radarsat-2 backscatter for bog (blue) and marsh (yellow) at (*a*) steep (25.7–27.6°) and (*b*) shallow (46.0–47.2°) incidence angles.

summer imagery as spring shallow imagery was not acquired). In the literature, steep-incidence angle imagery has been found to be best for differentiation between wetland vegetation types, particularly when vegetated areas are flooded, as there is increased backscatter at steep angles due to trunk–water double-bounce scattering and volume scattering among branches and other vegetation, such as reeds and grasses (Lu and Kwoun 2008; Baghdadi et al. 2001; Leckie and Ranson 1998). This was confirmed in this study as a result of differences in the vegetation structure. In spring, fens are typically comprised of short grass and sedge meadows with little water visibility to the radar pulse. Marshes typically had short, young, green growth as well as senescent, broken and horizontally lying (from snow load) reeds, which masked some of the standing water. Swamps were generally more open with large flooded areas and, where deciduous trees were present, they were either dead or their leaves had not yet flushed.

From the above, spring steep-angle imagery was determined to best distinguish the wetland classes. Analysis of wetland class discrimination was then conducted across all four study areas. Figure 8 shows spring steep-incidence angle backscatter values for all wetland types across all areas. Pairs of wetland types are displayed in separate graphs to

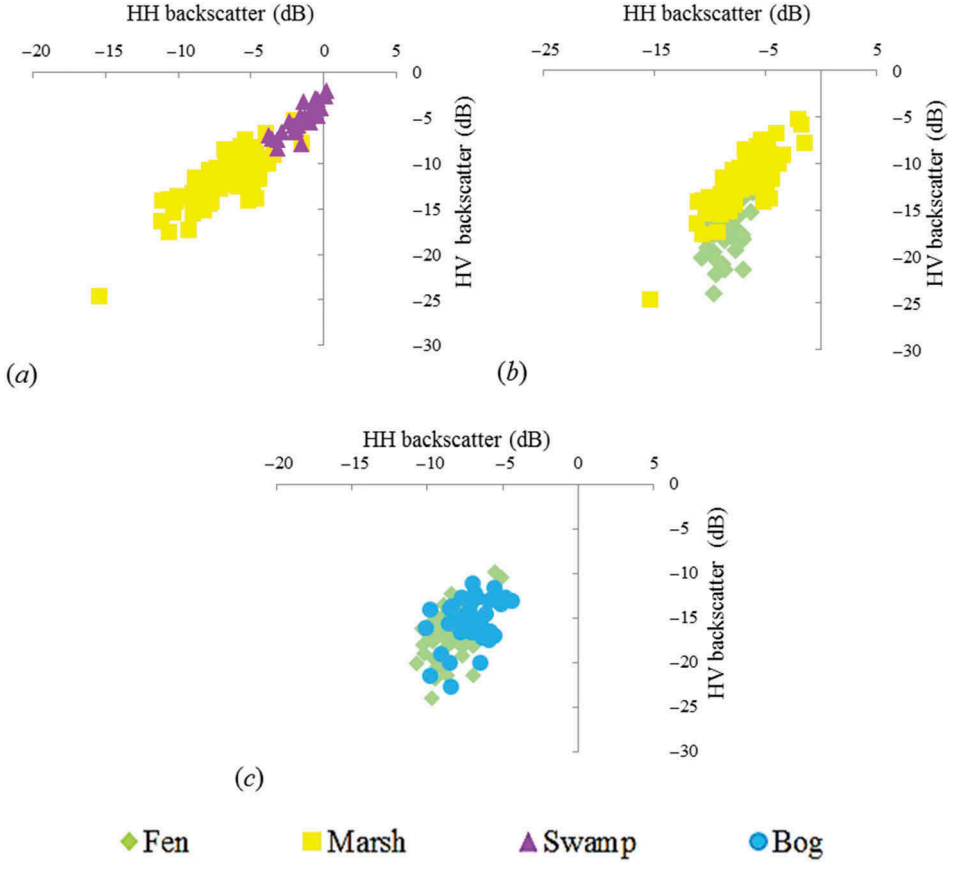

Figure 8. Spring 2010 Radarsat-2 backscatter for fen (green), marsh (yellow), swamp (purple), and bog (blue) at steep (18.4–27.6°) incidence angles with (*a*) marsh compared to swamp; (*b*) marsh compared to fen; and (*c*) fen compared to bog. Data are combined over all wetland study areas where the given classes were present.

allow clear comparisons; in the following discussion, refer to Figure 2(*a*)–(*d*) for visual representations of typical conditions for each wetland class. Swamp is distinct, for example, from marsh (Figure 8(*a*)) due to increased volume scattering in bare tree canopies and increased double-bounce scattering from bare trunks/branches and surrounding water. There would also be increased depolarization of the signal in swamp due to these multiple scattering interactions. There is more overlap between marsh and fen (Figure 8(*b*)), as expected, based upon the similarities in their vegetation structure (sedges, reeds, etc.). The most overlap is apparent for bog and fen (Figure 8(*c*)), which have the most similar types of vegetation. In the literature, bog has typically been shown to have lower HH backscatter than fen (e.g. in spring and summer, Radarsat-1, C-band imagery; e.g. Li and Chen 2005); however, in this study the vegetation composition and structure in bogs and fens were sufficiently similar to result in similar scattering properties at C-Band. Both had short vegetation with smooth canopies, albeit at bogs vegetation was mostly comprised of small bushes (Figure 2(*a*)) while fens were typically grassy meadows (Figure 2(*b*)). For this measurement and observation scale, configuration, and season, the differences between these types of canopies may be negligible with respect to C-band radar.

Among all study areas, the best separation between wetland type classes based upon backscatter was found using spring steep-angle imagery, and this concurs with most of the literature (e.g. Lu and Kwoun 2008; Baghdadi et al. 2001; Leckie and Ranson 1998). However, the high degree of overlap in backscatter between classes resulted in relatively poor overall CTA accuracies (40% at Westport to 65.0% at Loch Garry) when HH and HV backscatter intensities were used as the only input variables. The addition of HH and HV backscatter to the optical imagery spectral band brightness and DEM did not improve overall accuracies and caused large areas to be erroneously classified. For example, in Mer Bleue, large areas of the bog that were correctly classified using the optical/DEM data alone were erroneously classified as marsh when HH and HV backscatter were added as inputs; in Marlborough, large areas of various land cover types were erroneously classified as fen (e.g. Figure 9(*b*)) when backscatter was added.

Table 5 provides the classification accuracies for the four study areas as derived from spring WorldView-2, DEM, and spring steep-angle HH and HV backscatter data. The only class that showed improvement over all areas with the addition of HH and HV backscatter was swamp. Figure 9 provides a visual comparison of the Marlborough classifications, without (Figure 9(*a*)) and with (Figure 9(*b*)) HH and HV backscatter data as additional inputs. In the black circle of Figure 9(*b*), detail is lacking in an over-classified fen area. Figure 9(*a*) also over-estimates the amount of fen present there, but there is some detail representing the other classes. The red circle in Figure 9(*b*) shows an erroneously classified marsh that was correctly classified as fen in Figure 9(*a*). Despite these poorer results when radar backscatter was added as an input, Figure 9(*b*) shows better linear detail between farm fields in the northeastern corner, probably due to surface scattering within the bare fields in spring as compared with hedgerows between the fields with potential volume scattering and/or double-bounce scattering between the adjacent field and the woody hedgerow vegetation. Figure 9(*b*) also shows riverine marsh vegetation (blue circle) that represents a known creek (Steven's Creek) that is not as distinct in Figure 9(*a*).

5.2.1. *Integration of radar decomposition parameters in Wetland classification*

Cloude–Pottier entropy, anisotropy, and alpha components were derived from the spring steep-incidence angle Radarsat-2 imagery for all four study areas and used in object-

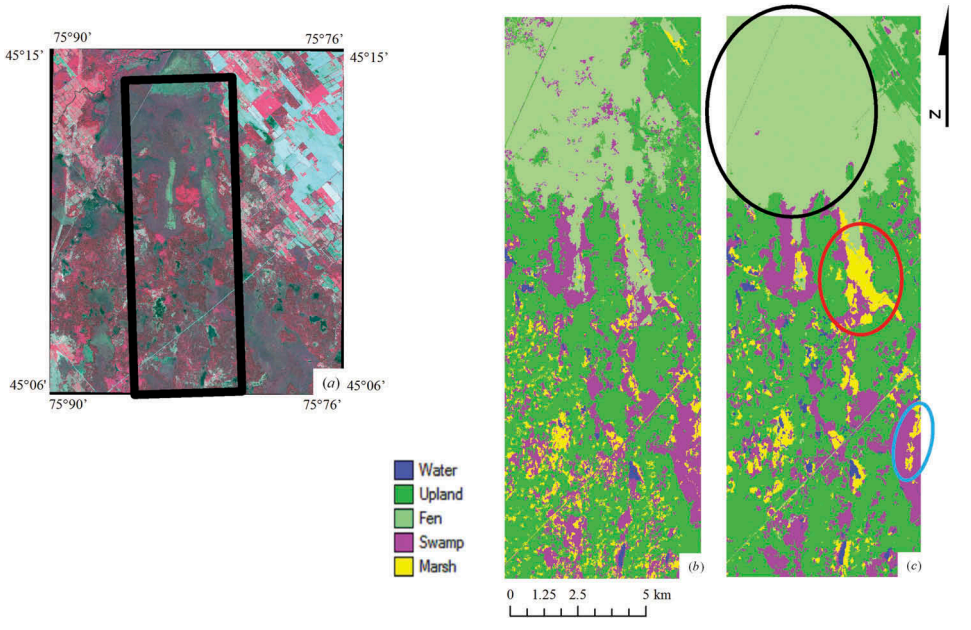

Figure 9. 2010 WorldView-2 CIR composite (*a*) and comparison of object-based CTA wetland classifications for the Marlborough study area using (*b*) spring WorldView-2 optical imagery and DEM; and (*c*) spring WorldView-2 optical imagery, DEM, and spring steep angle HH and HV backscatter images. Black circle shows over-classified fen. Red circle shows misclassified marsh. Blue circle shows well-delineated riverine feature.

based CTA wetland type classifications alone, and with the optical and DEM data. The results for the Marlborough wetland complex are presented here as an example. Figure 10(*a*) shows the spring WorldView-2 CIR composite and Figure 10(*b*)–(*d*) shows the three CP components. It can be seen in the entropy image that low values (e.g. certain fields as in the red circle) indicate that there was no significant mixing of scattering mechanisms, low depolarization, and a low degree of randomness, all typical of a relatively smooth surface.

Alpha identifies the dominant scattering mechanism and, as expected, low values (dark areas in the alpha image) occurred for water bodies (small ponds, red circles) indicating surface scattering. The brighter areas (red arrows) indicate double-bounce and volume scattering contributions. These areas are fen and mixed swamp, along with marsh. Fen typically had mostly surface scattering from the uniform grass and sedge cover but in the spring there were some contributions from double-bounce scattering due to the presence of run-off surface waters. Swamp in this area included significant proportions of dead coniferous and leaf-off deciduous trees, and therefore volume and double-bounce scattering would be expected, resulting in high alpha values and bright tones in the alpha image.

Anisotropy provides an indication of the mixing between the second and third scattering mechanisms, higher values (e.g. within the red circles) indicating that the second mechanism is dominant, which could relate again to the presence of water and stronger double-bounce scattering in the spring. However, in general the anisotropy image shows that two secondary mechanisms are mixed in about equal proportions (lower values).

Table 6 provides the overall classification accuracy results for the four study areas derived from the combined WorldView-2, DEM, and CP variables as inputs. The fen

Table 5. Accuracy statistics for object-based CTA using spring 2010 WorldView-2 imagery, DEM, and spring 2010 steep-angle Radarsat-2 HH and HV images at all four study areas. Values highlighted in orange show where there was improvement in classification over using optical imagery alone. Values highlighted in green show where there was a decline in accuracy with the addition of the backscatter images.

			Water		Upland		Fen		Bog		Swamp		Marsh		Average	
	Overall accuracy (%)	κ	PA (%)	UA (%)	PA (%)	UA (%)	PA (%)	UA (%)	PA (%)	UA (%)	PA (%)	UA (%)	PA (%)	UA (%)	PA (%)	UA (%)
Loch Garry	83.3	0.80	100.0	100.0	63.6	87.5	100.0	50.0	n/a	n/a	100.0	100.0	71.4	100.0	83.8	85.8
Marlborough	62.5	0.51	100.0	40.0	83.3	62.5	45.5	62.5	n/a	n/a	83.3	71.4	53.3	66.7	73.1	60.6
Mer Bleue	65.2	0.57	100.0	100.0	42.9	100.0	n/a	n/a	80.0	40.0	n/a	n/a	77.8	77.8	76.8	79.5
Westport	70.0	0.62	100.0	85.7	50.0	60.0	n/a	n/a	88.9	72.7	n/a	n/a	63.6	87.5	70.5	70.1
Average accuracy (%)	70.3	0.61	100.0	81.4	60.0	77.5	72.8	56.3	84.1	50.5	91.7	85.7	66.5	83.0		

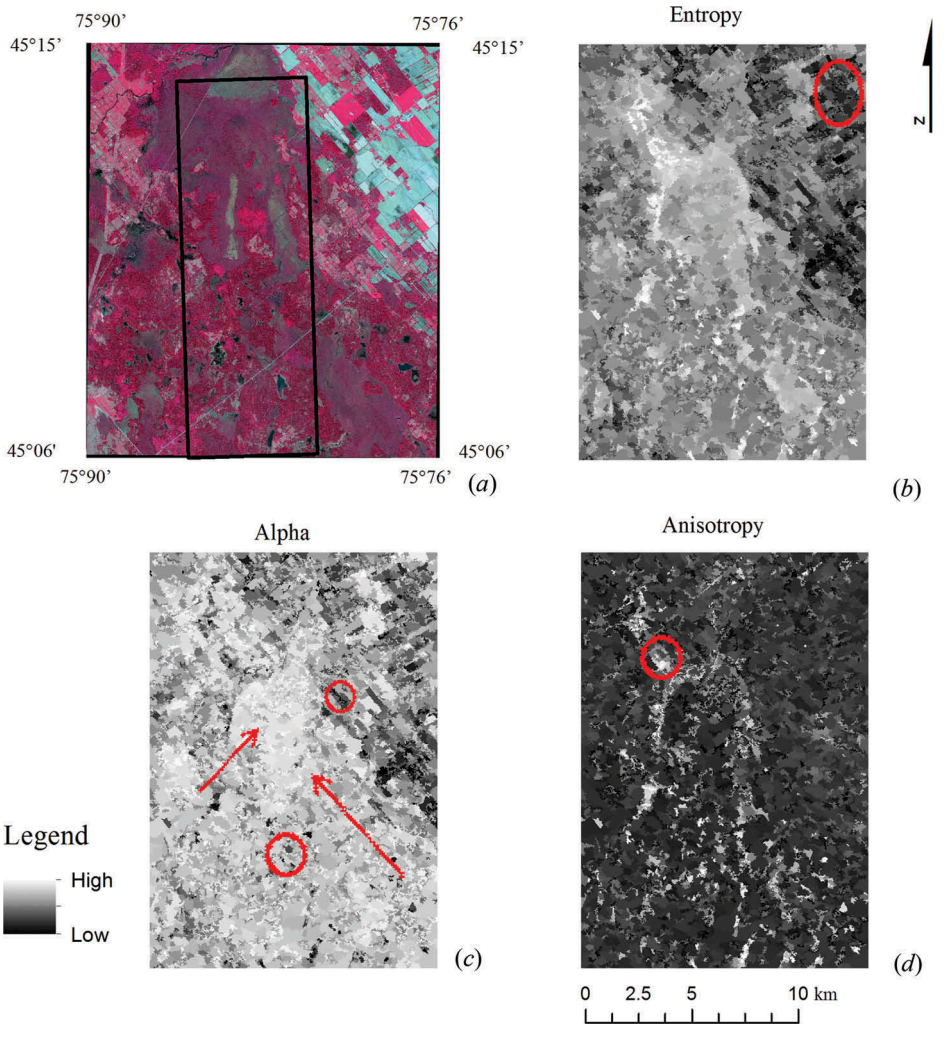

Figure 10. 2010 WorldView-2 CIR composite (*a*) and values of CP variables of (*b*) entropy, (*c*) alpha, and (*d*) anisotropy derived from 2010 spring steep-incidence angle Marlborough Radarsat-2 imagery. Red arrows and red circles denote examples of low and high values, respectively, of the CP variables.

class showed improvement with the addition of the CP variables at both study areas that contained fen. Table 7 provides a comparison summary of the average accuracies for each of the classification combinations; the best results averaged across all three combinations are highlighted in orange.

6. Discussion

This research found that object-based classification of wetland types benefitted from the complementary information in high-resolution optical and polarimetric radar data. Certain wetland classes were better discriminated using these combined data types than using either optical or radar data alone.

Table 6. Accuracy statistics for object-based CTA using spring 2010 WorldView-2 imagery, DEM, and spring 2010 steep-angle Radarsat-2 derived CP variables at all four study sites. Values highlighted in orange show where there was an improvement in classification over using optical imagery alone. Values highlighted in green show where there was a decline in accuracy with the addition of CP variables.

			Water		Upland		Fen		Bog		Swamp		Marsh		Average	
	Overall accuracy (%)	κ	PA (%)	UA (%)	PA (%)	UA (%)	PA (%)	UA (%)	PA (%)	UA (%)	PA (%)	UA (%)	PA (%)	UA (%)	PA (%)	UA (%)
Loch Garry	83.3	0.79	100.0	100.0	63.6	87.5	100.0	100.0	n/a	n/a	100.0	55.6	71.4	100.0	87.0	88.6
Marlborough	69.8	0.61	83.3	50.0	66.7	46.2	80.0	80.0	n/a	n/a	66.7	93.3	66.7	80.0	72.7	70.0
Mer Bleue	63.0	0.47	70.0	77.8	33.3	28.6	n/a	n/a	75.0	52.9	n/a	n/a	50.0	100.0	57.1	64.8
Westport	65.2	0.57	77.8	77.8	42.9	100.0	n/a	n/a	80.0	40.0	n/a	n/a	83.3	38.5	76.8	71.3
Average accuracy (%)	70.3	0.61	82.8	76.4	65.9	65.6	90.0	90.0	77.5	46.5	83.4	74.5	67.9	79.6		

Table 7. Summary of average accuracies (given as percentages, all areas) for each land cover type. Improvements with the addition of radar variables were found for the all but the marsh class.

	Water		Upland		Fen		Bog		Marsh		Swamp	
Optical plus DEM	95.8	93.7	68.8	84.8	90.0	75.0	65.9	50.3	66.2	83.0	80.0	61.3
Optical plus DEM plus HH, HV	100.0	81.4	60.0	77.5	72.8	56.3	84.1	50.5	66.5	83.0	91.7	85.7
Optical plus DEM plus CP	82.8	76.4	65.9	65.6	90.0	90.0	77.5	46.5	67.9	79.6	83.4	74.5

In evaluation of spring and summer C-band Radarsat-2 imagery at various incidence angles, steep-angle leaf-off spring imagery from March and April provided the best discrimination between swamp and other wetland types of marsh and fen. The swamp areas at Loch Garry were comprised of dead coniferous trees, while at Marlborough, many of the swamp areas were hardwood dominated. In spring, dead coniferous trees and leaf-off deciduous trees surrounded by standing water produced strong trunk-water double-bounce scattering along with volume scattering from crown branches and new understorey vegetation growth. This resulted in high backscatter, making them more distinct with the addition of backscatter in the classification than for the optical imagery alone. Kandus et al. (2001) found that leaf-off imagery (May and August in Argentina) best distinguished types of forest, marshes, and rushes. Lang, Townsend, and Kasischke (2008) found better discrimination for flooded forest during the leaf-off period in North Carolina.

Steep (18.4–27.6°) incidence angle HH and HV images showed better separation between wetland type classes than shallow (46.8–48.0°)-incidence angle HH and HV images. This is because for swamps and treed bogs, there was increased penetration at steep angles, increased volume scattering from branches within crowns, and double-bounce scattering between bare trunks and the water surface (particularly for swamps), resulting in increased depolarization of the signal. This concurs with the majority of the literature that has found that detection of flooded vegetation is better achieved with steep-incidence angle imagery (Westra et al. 2010; Li et al. 2007; McNairn et al. 2002; Baghdadi et al. 2001; Raney 1998).

Individual class accuracies for swamp improved using the combination of spring steep HH and HV images with the high-resolution WorldView-2 optical imagery at two of the four study areas (Loch Garry and Marlborough), and for bog at one study area (Westport). HH has often been shown to be sensitive to vegetation structure in a variety of studies with different radar sensors and locations, and for other non-wetland vegetation (such as agricultural vegetation) (Schmitt and Brisco 2013; Lang and Kasischke 2008; Pope et al. 1997).

Combining the CP variables derived from the steep-incidence angle radar imagery with optical imagery and a DEM did not increase overall accuracies over those obtained with optical/DEM data alone, with the exception of the fen class at Loch Garry and Marlborough. Scattering for fen is expected to be mostly surface scattering, with small contributions from volume scattering in shrub vegetation and double-bounce scattering where there are sporadic trees (e.g. tamarack in the Loch Garry fen) and open water and/or standing surface water. The fens at Marlborough were mostly grassy meadows. In the literature, it was found that CP components could distinguish between classes such as upland, wetland, forest, and shrub (Sartori et al. 2011) or that higher alpha values showed more double-bounce scattering in flooded vegetation compared with lower alpha values in non-flooded areas. In an alpha range of +20 to –20°, higher positive results (+14 to +20°) related to double-bounce, and lower negative results (–4 to –20°) related to surface scattering (Schmitt and Brisco 2013). In most of the wetlands of this study, surface scattering resulted in lower negative values.

The importance of optimal segmentation parameter selection is an ongoing aspect of interest in research using OBIA (Kloiber et al. 2015; Dronova et al. 2012; Dragut, Tiede, and Levick 2010; Marpu et al. 2010). As many studies utilize eCognition software to segment objects, additional, supportive evidence of the ‘correct’ scale (shape and compactness) values for particular imagery types is important. However, the choice of scale

parameter value is highly dependent upon the importance of particular features to the research, is related to the spatial resolution and spectral quality of the imagery being used, and is specific to eCognition (i.e. it is not easily generalized to other region-growing segmentation algorithms). Optimal segmentation of wetland types using WorldView-2 imagery and a DEM was achieved with a scale value of 45. This is similar to other wetland studies that used eCognition-based OBIA applied to high-resolution optical imagery. Examples include Dissanska, Bernier, and Payette (2009) using Quickbird imagery with a scale parameter value of 50, and Wang, Wang, and Zhou (2011) using IKONOS imagery and scale parameter values of 20 and 25.

6.1. Limitations and further research

The greatest overall limitation to this research was the size of the reference data set obtained in the field that was used for training and validation. The four wetland complexes were spatially dispersed and challenging to access. This, combined with the object-based classification approach, where a single area of a given wetland type can serve as only one sample value, resulted in low reference sample numbers. However, each sample spatially represented a much larger spatial extent (i.e. the extent of the segmented object) than would be represented by a single pixel in pixel-based classification, meaning there was spatially more information content within a given object reference sample than would be available using single pixel samples. Additionally, the individual site size was selected to represent 3 × 3 Landsat pixels as Landsat 5 TM data were used in the broader study described in Dingle Robertson (2014). In development of the fieldwork plan, all validation data requirements had to be weighed and the choice was made to visit field sites that could be utilized with all image data over visiting smaller individual sites for some of the data. Although the accuracy assessments were more comparable as the same samples were used for each data type, additional smaller validation sites would have allowed greater confidence in results from individual data types, such as the WorldView-2 imagery.

This research showed that there was variability in classifications of the wetland attributes that were specific to each wetland complex. This would not have been apparent with only one or two study areas: i.e. selection of the four different wetland complexes for this study was crucial in characterizing differences in ecology and vegetation composition and structure between the areas which resulted in different classification outcomes. In such research studies, a balance is necessary between the need for comprehensive validation sets and understanding of spatial differences across regions, but it is difficult to recommend a specific proportion for each.

Further research should incorporate a classification methodology (e.g. Random Forest (RF)) that determines the importance of the input optical and polarimetric radar variables to the overall classification. However, the drawback to simply using all the variables together is that there is a lack of understanding of the improvement or decline that each individual variable may cause, as was shown in this research. Additionally, in the determination of important data inputs RF can give the same (or higher) priority to highly correlated data (e.g. prioritizing them first) rather than ignoring correlated data, and shifting the prioritization to the other variables (Millard and Richardson 2013). Another potential benefit of a technique such as RF would be to offset the limitation of the small reference data set. By repeatedly parsing the reference set to different validation and training sets, the need for a large reference set is mitigated. This is important for areas such as wetlands where field access is difficult at best, and in many cases not possible.

7. Conclusions

The hypothesis of the research was that high-resolution spring season optical imagery, combined with a DEM and polarimetric radar image variables in OBIA, would provide improved discrimination of wetland classes over use of either optical/DEM or radar data alone. In determining the optimal radar data for classification, it was found that spring was better than summer season and that steep incidence angles were better than shallow incidence angles. Overall classification accuracy did not improve with the addition of the radar backscatter intensity and Cloude–Pottier decomposition variables to the optical/DEM data, but there was an improvement in specific wetland type classes of swamp, bog, and fen in some wetland complexes.

Disclosure statement

No potential conflict of interest was reported by the authors.

Funding

This research was funded by the Ontario Ministry of Natural Resources (C. Davies) and by an NSERC Discovery Grant to D. King. Radarsat-2 imagery and additional student funding were provided by the Landscape Science and Technology Division of Environment Canada.

References

Adam, E., O. Mutanga, and D. Rugege. 2010. "Multispectral and Hyperspectral Remote Sensing for Identification and Mapping of Wetland Vegetation: A Review." *Wetlands Ecology and Management* 18: 281–296. doi:10.1007/s11273-009-9169-z.

Aguilar, M. A., M. M. Saldana, and F. J. Aguilar. 2013. "Geoeye-1 and Worldview-2 Pan-Sharpened Imagery for Object-Based Classification in Urban Environments." *International Journal of Remote Sensing* 34: 2583–2606. doi:10.1080/01431161.2012.747018.

Apte, C., and S. Weiss. 1997. "Data Mining with Decision Trees and Decision Rules." *Future Generation Computer Systems* 13: 197–210. doi:10.1016/S0167-739X(97)00021-6.

Baghdadi, N., M. Bernier, R. Gauthier, and I. Neeson. 2001. "Evaluation of C-Band SAR Data for Wetlands Mapping." *International Journal of Remote Sensing* 22: 71–88. doi:10.1080/014311601750038857.

Banks, S. N., D. J. King, A. Merzouki, and J. Duffe. 2014. "Characterizing Scattering Behaviour and Assessing Potential for Classification of Arctic Shore and Near-Shore Land Covers with Fine Quad-Pol RADARSAT-2 Data." *Canadian Journal of Remote Sensing* 40: 291–314. doi:10.1080/07038992.2014.979487.

Belluco, E., M. Camuffo, S. Ferrari, L. Modenese, S. Silvestri, A. Marani, and M. Marani. 2006. "Mapping Salt-Marsh Vegetation by Multispectral and Hyperspectral Remote Sensing." *Remote Sensing of Environment* 105: 54–67. doi:10.1016/j.rse.2006.06.006.

Bernier, M., H. Ghedira, Y. Gauthier, R. Magagi, R. Filion, D. De Seve, T. B. M. J. Ouarda, J.-P. Villeneuve, and P. Buteau. 2003. "Détection Et Classification De Tourbières Ombrotrophes Du Québec À Partir D'images RADARSAT-1." *Canadian Journal of Remote Sensing* 29: 88–98. doi:10.5589/m02-083.

Boerner, W. M., H. Mott, E. Luneburg, C. Livingstone, B. Brisco, R. J. Brown, and J. S. Paterson. 1998, "Polarimetry in Radar Remote Sensing: Basic and Applied Concepts." In *Principles and Applications of Imaging Radar: Manual of Remote Sensing*. Vol. 2. 3rd ed., edited by R. M. Henderson and A. J. Lewis. New York, NY: John Wiley and Sons.

Brenner, J. C., Z. Christman, and J. Rogan. 2012. "Segmentation of Landsat Thematic Mapper Imagery Improves Buffelgrass (*Pennisetum Ciliare)* Pasture Mapping in the Sonoran Desert of Mexico." *Applied Geography* 34: 569–575. doi:10.1016/j.apgeog.2012.02.008.

Burnett, C., and T. Blaschke. 2003. "A Multi-Scale Segmentation/Object Relationship Modelling Methodology for Landscape Analysis." *Ecological Modelling* 168: 233–249. doi:10.1016/S0304-3800(03)00139-X.

Castaneda, C., and D. Ducrot. 2009. "Land Cover Mapping of Wetland Areas in an Agricultural Landscape Using SAR and Landsat Imagery." *Journal of Environmental Management* 90: 2270–2277. doi:10.1016/j.jenvman.2007.06.030.

Cloude, S. R., and E. Pottier. 1996. "A Review of Target Decomposition Theorems in Radar Polarimetry." *IEEE Transactions on Geoscience and Remote Sensing* 34: 498–518. doi:10.1109/36.485127.

Cloude, S. R., and E. Pottier. 1997. "An Entropy Based Classification Scheme for Land Applications of Polarimetric SAR." *IEEE Transactions on Geoscience and Remote Sensing* 35: 68–78. doi:10.1109/36.551935.

Congalton, R. G., and K. Green. 1993. "A Practical Look at the Sources of Confusion in Error Matrix Generation." *Photogrammetric Engineering and Remote Sensing* 59: 641–644.

Dabrowska-Zielinska, K., M. Gruszczynska, S. Lewinski, A. Hoscilo, and J. Bojanowski. 2009. "Application of Remote and *in situ* Information to the Management of Wetlands in Poland." *Journal of Environmental Management* 90: 2261–2269. doi:10.1016/j.jenvman.2008.02.009.

De Leeuw, M. R. 2009. "Performance Evaluation of Several Adaptive Speckle Filters for SAR Imaging." Paper presented at Anais XIV Simposio Brasileiro de Sensoriamento Remoto, 7299–7305, Natal, Brasil, INPE, April 25–30.

Dillabaugh, K. A., and D. J. King. 2008. "Riparian Marshland Composition and Biomass Mapping Using Ikonos Imagery." *Canadian Journal of Remote Sensing* 34: 143–158. doi:10.5589/m08-011.

Dingle Robertson, L. 2014. "Evaluating Spatial and Seasonal Variability of Wetlands in Eastern Ontario using Remote Sensing and GIS." PhD diss., Carleton University, Ottawa, Canada. 428 pp.

Dingle Robertson, L., and D. J. King. 2011. "Comparison of Pixel- and Object-Based Classification in Land Cover Change Mapping." *International Journal of Remote Sensing* 32: 1505–1529. doi:10.1080/01431160903571791.

Dissanska, M., M. Bernier, and S. Payette. 2009. "Object-Based Classification of Very High Resolution Panchromatic Images for Evaluating Recent Change in the Structure of Patterned Peatlands." *Canadian Journal of Remote Sensing* 35: 189–215. doi:10.5589/m09-002.

Dobson, M. C., and F. T. Ulaby. 1988. "Active Microwave Soil Moisture Research." *IEEE Transactions on Geoscience and Remote Sensing* GE24: 23–36.

Dragut, L., D. Tiede, and S. R. Levick. 2010. "ESP: A Tool to Estimate Scale Parameter for Multiresolution Image Segmentation of Remotely Sensed Data." *International Journal of Geographical Information Science* 24: 859–871. doi:10.1080/13658810903174803.

Dribault, Y., K. Chokmani, and M. Bernier. 2012. "Monitoring Seasonal Hydrological Dynamics of Minerotrophic Peatlands Using Multi-Date Geoeye-1 Very High Resolution Imagery and Object-Based Classification." *Remote Sensing* 4: 1887–1912. doi:10.3390/rs4071887.

Dronova, I., P. Gong, N. E. Clinton, L. Wang, W. Fu, S. Qi, and Y. Liu. 2012. "Landscape Analysis of Wetland Plant Functional Types: The Effects of Image Segmentation Scale, Vegetation Classes, and Classification Methods." *Remote Sensing of Environment* 127: 357–369. doi:10.1016/j.rse.2012.09.018.

Dronova, I., P. Gong, and L. Wang. 2011. "Object-Based Analysis and Change Detection of Major Wetland Cover Types and Their Classification Uncertainty during the Low Water Period at Poyang Lake, China." *Remote Sensing of Environment* 115: 3220–3236. doi:10.1016/j.rse.2011.07.006.

Durieux, L., J. Kropáček, G. D. De Grandi, and F. Achard. 2007. "Object-Oriented and Textural Image Classification of the Siberia GBFM Radar Mosaic Combined with MERIS Imagery for Continental Scale Land Cover Mapping." *International Journal of Remote Sensing* 28: 4175–4182. doi:10.1080/01431160701236837.

Duro, D. C., S. E. Franklin, and M. G. Dube. 2012. "A Comparison of Pixel-Based and Object-Based Image Analysis with Selected Machine Learning Algorithms for the Classification of Agricultural Landscapes Using SPOT-5 HRG Imagery." *Remote Sensing of Environment* 118: 259–272. doi:10.1016/j.rse.2011.11.020.

Evans, D. L., T. G. Farr, J. J. Van Zyl, and H. A. Zebker. 1988. "Radar Polarimetry: Analysis Tools and Applications." *IEEE Transactions on Geoscience and Remote Sensing* 26: 774–789. doi:10.1109/36.7709.

Evans, T. L., and M. Costa. 2013. "Landcover Classification of the Lower Nhecolândia Subregion of the Brazilian Pantanal Wetlands Using ALOS/PALSAR, RADARSAT-2 and ENVISAT/ASAR Imagery." *Remote Sensing of Environment* 128: 118–137. doi:10.1016/j.rse.2012.09.022.

Evans, T. L., M. Costa, W. M. Tomas, and A. R. Camilo. 2014. "Large-Scale Habitat Mapping of the Brazilian Pantanal Wetland: A Synthetic Aperture Radar Approach." *Remote Sensing of Environment* 155: 89–108. doi:10.1016/j.rse.2013.08.051.

Foody, G. M. 2002. "Status of Land Cover Classification Accuracy Assessment." *Remote Sensing of Environment* 80: 185–201. doi:10.1016/S0034-4257(01)00295-4.

Friedl, M. A., and C. E. Brodley. 1997. "Decision Tree Classification of Land Cover from Remotely Sensed Data." *Remote Sensing of Environment* 61: 399–409. doi:10.1016/S0034-4257(97)00049-7.

Grenier, M., A.-M. Demers, S. Labrecque, M. Benoit, R. A. Fournier, and B. Drolet. 2007. "An Object-Based Method to Map Wetland Using RADARSAT-1 and Landsat ETM Images: Test Case on Two Sites in Quebec, Canada." *Canadian Journal of Remote Sensing* 33: S28–S45. doi:10.5589/m07-048.

Henderson, F. M., and A. J. Lewis. 2008. "Radar Detection of Wetland Ecosystems: A Review." *International Journal of Remote Sensing* 29: 5809–5835. doi:10.1080/01431160801958405.

Horritt, M. S., D. C. Mason, D. M. Cobby, I. J. Davenport, and P. D. Bates. 2003. "Waterline Mapping in Flooded Vegetation from Airborne SAR Imagery." *Remote Sensing of Environment* 85: 271–281. doi:10.1016/S0034-4257(03)00006-3.

Jiao, Z., C. Woodcock, C. B. Schaaf, B. Tan, J. Liu, F. Gao, A. Strahler, X. Li, and J. Wang. 2011. "Improving MODIS Land Cover Classification by Combining MODIS Spectral and Angular Signatures in a Canadian Boreal Forest." *Canadian Journal of Remote Sensing* 37: 184–203. doi:10.5589/m11-030.

Kandus, P., H. Karszenbaum, T. Pultz, G. Parmuchi, and J. Bava. 2001. "Influence of Flood Conditions and Vegetation Status on the Radar Backscatter of Wetland Ecosystems." *Canadian Journal of Remote Sensing* 27: 651–662. doi:10.1080/07038992.2001.10854907.

Karszenbaum, H., P. Kandus, M. Martinez, T. Le Toan, J. Tiffenberg, and M. G. Parmuchi. 2000. *ERS-2, RADARSAT SAR Backscattering Characteristics of the Paraná River Delta Wetland, Argentina*. Noordwijk: European Space Agency, Special Publication, SP-461.

Kasischke, E. S., J. M. Melack, and M. C. Dobson. 1997. "The Use of Imaging Radars for Ecological Applications – a Review." *Remote Sensing of Environment* 59: 141–156. doi:10.1016/S0034-4257(96)00148-4.

Keddy, C. 1995. *The Conservation Potential of the Frontenac Axis: Linking Algonquin Park to the Adirondacks*, 59. Ottawa Valley: The Canadian Parks and Wilderness Society.

Kloiber, S. M., R. D. Macleod, A. J. Smith, J. F. Knight, and B. J. Huberty. 2015. "A Semi-Automated, Multi-Source Data Fusion Update of A Wetland Inventory for East-Central Minnesota, USA." *Wetlands*, January 2015. Online Publication.

Laliberte, A. S., A. Rango, K. M. Havstad, J. F. Paris, R. F. Beck, R. McNeely, and A. L. Gonzalez. 2004. "Object-Oriented Image Analysis for Mapping Shrub Encroachment from 1937 to 2003 in Southern New Mexico." *Remote Sensing of Environment* 93: 198–210. doi:10.1016/j.rse.2004.07.011.

Lang, M. W., and E. S. Kasischke. 2008. "Using C-Band Synthetic Aperture Radar Data to Monitor Forested Wetland Hydrology in Maryland's Coastal Plain, USA." *IEEE Transactions on Geoscience and Remote Sensing* 46: 535–546. doi:10.1109/TGRS.2007.909950.

Lang, M. W., P. A. Townsend, and E. S. Kasischke. 2008. "Influence of Incidence Angle on Detecting Flooded Forests Using C-HH Synthetic Aperture Radar Data." *Remote Sensing of Environment* 112: 3898–3907. doi:10.1016/j.rse.2008.06.013.

Leckie, D. G., and K. J. Ranson. 1998, "Forestry Applications Using Imaging Radar." In *Principles and Applications of Imaging Radar: Manual of Remote Sensing*. Vol. 2. 3rd ed., edited by R. M. Henderson and A. J. Lewis. New York, NY: John Wiley and Sons.

Li, G., D. Lu., E. Moran, L. Dutra, and M. Batistella. 2012. "A Comparative Analysis of ALOS PALSAR L-Band and RADARSAT-2 C-Band Data for Land-Cover Classification in A Tropical Moist Region." *ISPRS Journal of Photogrammetry and Remote Sensing* 70: 26–38. doi:10.1016/j.isprsjprs.2012.03.010.

Li, J., and W. Chen. 2005. "A Rule-Based Method for Mapping Canada's Wetlands Using Optical, Radar and DEM Data." *International Journal of Remote Sensing* 26: 5051–5069. doi:10.1080/01431160500166516.

Li, X., A. Gar-On Yeh, S. Wang, K. Liu, X. Liu, J. Qian, and X. Chen. 2007. "Regression and Analytical Models for Estimating Mangrove Wetland Biomass in South China Using Radarsat Images." *International Journal of Remote Sensing* 28: 5567–5582. doi:10.1080/01431160701227638.

Liao, J., and Q. Wang. 2010. "Wetland Characterization and Classification Using Polarimetric Radarsat-2 Data." In *the Proceedings of SPIE*. Vol. 7841, edited by H. Guo and C. Wang. Sixth International Symposium on Digital Earth: Data Processing and Applications. SPIE, Digital Library. http://dx.doi.org/10.1117/12.873258

Lu, Z., and O.-I. Kwoun. 2008. "Radarsat-1 and ERS Insar Analysis over Southeastern Coastal Louisiana: Implications for Mapping Water-Level Changes beneath Swamp Forests." *IEEE Transactions on Geoscience and Remote Sensing* 46: 2167–2184. doi:10.1109/TGRS.2008.917271.

Marechal, C., E. Pottier, L. Hubert-Moy, and S. Rapinel. 2012. "One Year Wetland Survey Investigations from Quad-Pol RADARSAT-2 Time-Series SAR Images." *Canadian Journal of Remote Sensing* 38: 240–252. doi:10.5589/m12-017.

Marpu, P. R., M. Neubert, H. Herold, and I. Niemeyer. 2010. "Enhanced Evaluation of Image Segmentation Results." *Journal of Spatial Science* 55: 55–68. doi:10.1080/14498596.2010.487850.

Marti-Cardona, B., T. D. Tran, E. Blade-Castellet, and J. Dolz-Ripolles. 2010. "ASAR/ENVISAT Images for the Calibration of Wind Hydrodynamic Effect on Donana Wetlands." *IAHS-AISH Publication* 352: 459–463.

McCoy, R. M. 2005. *Field Methods in Remote Sensing*. New York, NY: Guildford Press.

McNairn, H., C. Duguay, B. Brisco, and T. J. Pultz. 2002. "The Effect of Soil and Crop Residue Characteristics on Polarimetric Radar Response." *Remote Sensing of Environment* 80: 308–320. doi:10.1016/S0034-4257(01)00312-1.

Meneguzzo, D. M., G. C. Liknes, and M. D. Nelson. 2013. "Mapping Trees outside Forests Using High-Resolution Aerial Imagery: A Comparison of Pixel- and Object-Based Classification Approaches." *Environmental Monitoring and Assessment* 185: 6261–6275. doi:10.1007/s10661-012-3022-1.

Millard, K., and M. Richardson. 2013. "Wetland Mapping with Lidar Derivatives, SAR Polarimetric Decompositions and Lidar-SAR Fusion Using a Random Forest Classifier." *Canadian Journal of Remote Sensing* 39: 290–307. doi:10.5589/m13-038.

Moffett, K. B., and S. M. Gorelick. 2013. "Distinguishing Wetland Vegetation and Channel Features with Object-Based Image Segmentation." *International Journal of Remote Sensing* 34: 1332–1354. doi:10.1080/01431161.2012.718463.

Muster, S., B. Heim, A. Abnizova, and J. Boike. 2013. "Water Body Distributions Across Scales: A Remote Sensing Based Comparison of Three Arctic TundraWetlands." *Remote Sensing* 5: 1498–1523. doi:10.3390/rs5041498.

Mutanga, O., E. Adam, and M. A. Cho. 2012. "High Density Biomass Estimation for Wetland Vegetation Using Worldview-2 Imagery and Random Forest Regression Algorithm." *International Journal of Applied Earth Observation and Geoinformation* 18: 399–406. doi:10.1016/j.jag.2012.03.012.

Mwita, E., G. Menz, S. Misana, M. Becker, D. Kisanga, and B. Boehme. 2013. "Mapping Small Wetlands of Kenya and Tanzania Using Remote Sensing Techniques." *International Journal of Applied Earth Observation and Geoinformation* 21: 173–183. doi:10.1016/j.jag.2012.08.010.

National Wetlands Working Group. 1997. *The Canadian Wetland Classification System*. 2nd ed. Edited by B. G. Warner and C. D. A. Rubec, 68p. Waterloo, ON: Wetlands Research Centre, University of Waterloo.

Ouyang, Z.-T., M.-Q. Zhang, X. Xie, Q. Shen, H.-Q. Guo, and B. Zhao. 2011. "A Comparison of Pixel-Based and Object-Oriented Approaches to VHR Imagery for Mapping Saltmarsh Plants." *Ecological Informatics* 6: 136–146. doi:10.1016/j.ecoinf.2011.01.002.

Ozesmi, S. L., and M. E. Bauer. 2002. "Satellite Remote Sensing of Wetlands." *Wetlands Ecology and Management* 10: 381–402. doi:10.1023/A:1020908432489.

Pasher, J., S. W. Mitchell, D. J. King, L. Fahrig, A. C. Smith, and K. E. Lindsay. 2013. "Optimizing Landscape Selection for Estimating Relative Effects of Landscape Variables on Ecological Responses." *Landscape Ecology* 28: 371–383. doi:10.1007/s10980-013-9852-6.

Pope, K. O., E. Rejmankova, J. F. Paris, and R. Woodruff. 1997. "Detecting Seasonal Flooding Cycles in Marshes of the Yucatan Peninsula with SIR-C Polarimetric Radar Imagery." *Remote Sensing of Environment* 59: 157–166. doi:10.1016/S0034-4257(96)00151-4.

Quinlan, J. R. 1990. "Decision Trees and Decision Making." *IEEE Transactions on Systems. Man. and Cybernetics* 20: 339–346. doi:10.1109/21.52545.

Racine, M.-J., M. Bernier, and T. Ouarda. 2005. "Evaluation of RADARSAT-1 Images Acquired in Fine Mode for the Study of Boreal Peatlands: A Case Study in James Bay, Canada." *Canadian Journal of Remote Sensing* 31: 450–467. doi:10.5589/m05-029.

Ramsar (Ramsar Convention Secretariat). 2006. *The Ramsar Convention Manual: A guide to the Convention on Wetlands (Ramsar, Iran, 1971)*. 4th ed., 114p. Gland, Switzerland: Ramsar Convention Secretariat.

Raney, R. K. 1998, "Radar Fundamentals: Technical Perspective." In *Principles and Applications of Imaging Radar: Manual of Remote Sensing*. Vol. 2. 3rd ed., edited by R. M. Henderson and A. J. Lewis. New York, NY: John Wiley and Sons.

Ricaurte, L. F., J. Jokela, A. Siqueira, M. Núñez-Avellaneda, C. Marin, A. Velázquez-Valencia, and K. M. Wantzen. 2012. "Wetland Habitat Diversity in the Amazonian Piedmont of Colombia." *Wetlands* 32: 1189–1202. doi:10.1007/s13157-012-0348-y.

Rivero, R. G., S. Grunwald, M. W. Binford, and T. Z. Osborne. 2009. "Integrating Spectral Indices into Prediction Models of Soil Phosphorus in a Subtropical Wetland." *Remote Sensing of Environment* 113: 2389–2402.

Sartori, L. R., N. N. Imai, J. C. Mura, E. Leao De Moraes Novo, and T. S. F. Silva. 2011. "Mapping Macrophyte Species in the Amazon Floodplain Wetlands Using Fully Polarimetric ALOS/PALSAR Data." *IEEE Transactions on Geoscience and Remote Sensing* 49: 4717–4728.

Schmitt, A., and B. Brisco. 2013. "Wetland Monitoring Using the Curvelet-Based Change Detection Method on Polarimetric SAR Imagery." *Water* 5: 1036–1051. doi:10.3390/w5031036.

Silva, T. S. F., M. P. F. Costa, and J. M. Melack. 2010. "Spatial and Temporal Variability of Macrophyte Cover and Productivity in the Eastern Amazon Floodplain: A Remote Sensing Approach." *Remote Sensing of Environment* 114: 1998–2010.

Silva, T. S. F., M. P. F. Costa, J. M. Melackm, and E. M. L. M. Novo. 2008. "Remote Sensing of Aquatic Vegetation: Theory and Applications." *Environmental Monitoring and Assessment* 140: 131–145. doi:10.1007/s10661-007-9855-3.

Tian, J., and D.-M. Chen. 2007. "Optimization in Multi-Scale Segmentation of High-Resolution Satellite Images for Artificial Feature Recognition." *International Journal of Remote Sensing* 28: 4625–4644. doi:10.1080/01431160701241746.

Touzi, R., W. M. Boerner, J. S. Lee, and E. Luneburg. 2004. "A Review of Polarimetry in the Context of Synthetic Aperture Radar: Concepts and Information Extraction." *Canadian Journal of Remote Sensing* 30: 380–407.

Touzi, R., A. Deschamps, and G. Rother. 2007. "Wetland Characterization Using Polarimetric RADARSAT-2 Capability." *Canadian Journal of Remote Sensing* 33: S56–S67. doi:10.5589/m07-047.

Ulaby, F. T., T. F. Haddock, and R. T. Austin. 1988. "Fluctuation Statistics of Millimeter-Wave Scattering from Distributed Targets." *IEEE Transactions on Geoscience and Remote Sensing* 26: 268–281.

Van Beijma, S., A. Comber, and A. Lamb. 2014. "Random Forest Classification of Salt Marsh Vegetation Habitats Using Quad-Polarimetric Airborne SAR, Elevation and Optical RS Data." *Remote Sensing of Environment* 149: 118–129.

Van Zyl, J. J., H. A. Zebker, and C. Elachi. 1987. "Imaging Radar Polarisation Signatures: Theory and Observation." *Radio Science* 22: 52–543.

Waleska, S., P. Rodrigues, P. Walfir, and M. Souza-Filho. 2011. "Use of Multi-Sensor Data to Identify and Map Tropical Coastal Wetlands in the Amazon of Northern Brazil." *Wetlands* 31: 11–23.

Wang, X., K. Wang, and B. Zhou. 2011. "Object-Based Classification of IKONOS Data for Endemic Torreya Mapping." *Procedia Environmental Sciences* 10: 1887–1891. doi:10.1016/j.proenv.2011.09.295.

Westra, T., R. De Wulf, F. Van Coillie, and S. Crabbe. 2010. "Optimal ENVISAT Advanced Synthetic Aperture Radar Image Parameters for Mapping and Monitoring Sahelian Floodplains." *Journal of Applied Remote Sensing* 4: 1–17.

Wright, C., and A. Gallant. 2007. "Improved Wetland Remote Sensing in Yellowstone National Park Using Classification Trees to Combine TM Imagery and Ancillary Environmental Data." *Remote Sensing of Environment* 107: 582–605.

Zambon, M., R. Lawrence, A. Bunn, and S. Powell. 2006. "Effect of Alternative Splitting Rules on Image Processing Using Classification Tree Analysis." *Photogrammetric Engineering & Remote Sensing* 72: 25–30. doi:10.14358/PERS.72.1.25.

Zhang, H., D. Li, L. Li, and A. Shi. 2011. "Wetland Landscape Pattern Analysis with Remote Sensing Images in Ximen Island Special Marine Protected Area." In *Proceedings of SPIE 8181*, edited by U. Michel and D. L. Civco. Earth Resources and Environmental Remote Sensing/GIS Applications II conference, October 27. SPIE. doi:10.1117/12.897709.